

Electronic Supplementary Information for

3D Porous Metal–Organic Framework for Selective Adsorption of Methane over Dinitrogen under Ambient Pressure

Charlie E. Kivi, Benjamin S. Gelfand, Hana Dureckova, Ha T. K. Ho, Cindy Ma, George K. H. Shimizu, Tom K. Woo, and Datong Song

1	General Considerations	S1
2	Synthesis	S1
2.1	Synthesis of 3,5-dimethylpyrazole-4-carboxylic acid ethyl ester (I).....	S1
2.2	Synthesis of diethyl 1,1'-methylenebis(3,5-dimethyl-1H-pyrazole-4-carboxylate) (II) ..	S2
2.3	Synthesis of 1,1'-methylenebis(3,5-dimethyl-1H-pyrazolyl-4-carboxylic acid) (H₂L) ...	S3
2.4	Synthesis of [NiL] _n ·xDMO (1)	S4
3	Single Crystal X-Ray Diffraction.....	S5
3.1	Methods.....	S5
3.2	Single Crystal Properties.....	S5
4	Thermogravimetric Analysis, Powder X-Ray, and IR	S7
5	Gas Sorption.....	S8
5.1	Adsorption Analysis.....	S8
5.2	Surface Area.....	S9
5.3	Isosteric Heat of Adsorption Calculation.....	S10
5.4	Selectivity	S13
5.5	Selectivity and Working Capacity Comparison of 1 versus other Literature Materials .	S14
5.6	Post Adsorption Stability	S15
6	Stability of 1	S15
6.1	Chemostability of 1	S15
6.2	Thermal stability of 1	S15
7	Computational Details and Observed CH ₄ and N ₂ Sites of Adsorption in 1	S17
8	References	S18

1 General Considerations

Elemental analyses were performed on a Thermo Flash 2000 CHN analyzer. Thermogravimetric analyses (TGA) were performed on a TA Instruments SDT Q600 instrument under a nitrogen atmosphere with a heating rate of 5 °C per minute in an alumina sample pan with an empty pan as the reference. NMR spectra were recorded on a Bruker Avance 400 spectrometer. Both ^1H and ^{13}C NMR spectra were referenced and reported relative to the solvent signals. Powder X-ray diffraction (PXRD) experiments were performed on a Rigaku MiniFlex 600 diffractometer equipped with a Cu-K α source operating at 40 kV and 15 mA at the Walter Curlook Materials Characterization & Processing Laboratory, Department of Materials Science and Engineering, University of Toronto. A step scan mode was used for data acquisition with a step size of $0.02^\circ 2\theta$. PXRD samples for characterization were prepared by dropcasting the acetone suspensions onto a silicon zero background sample holder. Infrared spectrum was recorded using a neat sample on a Bruker Alpha FT-IR spectrometer equipped with a Platinum ATR sampling unit in air. Adsorption isotherms were conducted using an Accelerated Surface Area & Porosimetry System (ASAP) 2020 supplied by Micromeritics Instruments Inc. Variable temperature PXRD was conducted on a Bruker D8 Advance Eco equipped with a variable temperature MTC-HIGHTEMP sample stage with a Cu-K α source. A step scan mode was used for data acquisition with a step size of $0.025^\circ 2\theta$ with a heating rate of 300 °C per minute. Samples were prepared on an inert PtRh strip. All reagents were purchased from commercial sources and used without further purification. Ethyl diacetylacetate was prepared following literature procedures.¹

2 Synthesis

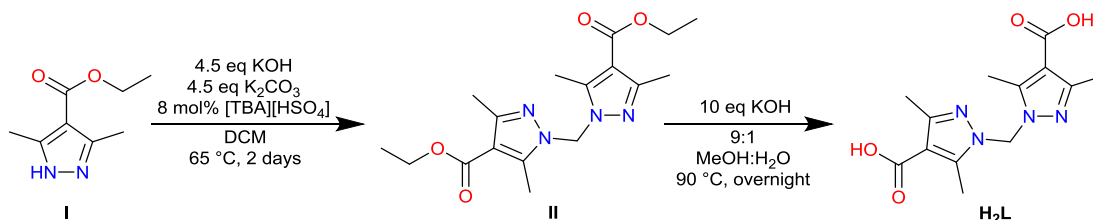


Figure S1: Synthesis of ligand H₂L.

2.1 Synthesis of 3,5-dimethylpyrazole-4-carboxylic acid ethyl ester (I)

In a modification of literature procedures,² ethyl diacetylacetate (25.0 g, 145 mmol) was dissolved in 290 mL of methanol in a 0 °C ice bath. 12 M hydrochloric acid (1.5 mL, 18 mmol) was added to the solution and stirred for 20 min. Hydrazine monohydrate (17.5 mL, 359 mmol) was added dropwise to the solution after which the flask was allowed to slowly warm to room temperature overnight. After stirring, the methanol was removed under reduced pressure and 100 mL of water was introduced to induce precipitation white solids. The solids were collected by vacuum filtration,

washed with water (5 x 20 mL), and air dried. The crude product was dissolved in dichloromethane (DCM) and filtered through silica gel. After the removal of DCM under reduced pressure, 20 g of white solids (81% yield) were obtained. Spectroscopic data matches the literature data.

2.2 Synthesis of diethyl 1,1'-methylenebis(3,5-dimethyl-1H-pyrazole-4-carboxylate) (II)

Following literature procedures,³ **I** (10.0 g, 59.5 mmol) was added to freshly ground KOH (15.0 g, 268 mmol), potassium carbonate (37.0 g, 268 mmol) and tetra-*n*-butylammonium hydrogen sulfate (1.62 g, 4.76 mmol) in DCM (400 mL). The solution was refluxed at 65 °C 3 days until it assumed a deep orange colour. The solution was washed once with water (~400 mL) and four times with brine (~200 mL). The collected organic phase was dried over magnesium sulfate, filtered and dried under vacuum for 3 days to yield 9.68 g (93% yield) of white solids, which were used without further purification. Crystals suitable for X-ray crystallography were obtained via the slow diffusion of pentane into a chloroform solution. ¹H NMR (400 MHz, CDCl₃) δ 6.10 (s, 2H), 4.26 (q, J = 7.1 Hz, 4H), 2.73 (s, 6H), 2.37 (s, 6H), 1.33 (t, J = 7.1 Hz, 6H). ¹³C NMR (101 MHz, CDCl₃) δ 164.36, 151.50, 145.89, 111.06, 60.09, 59.91, 14.51, 14.44, 11.56. Anal. Calcd. for C₁₇H₂₄N₄O₄: C 58.61, H 6.94, N 16.08; found C 58.50, H 6.92, N 16.14.

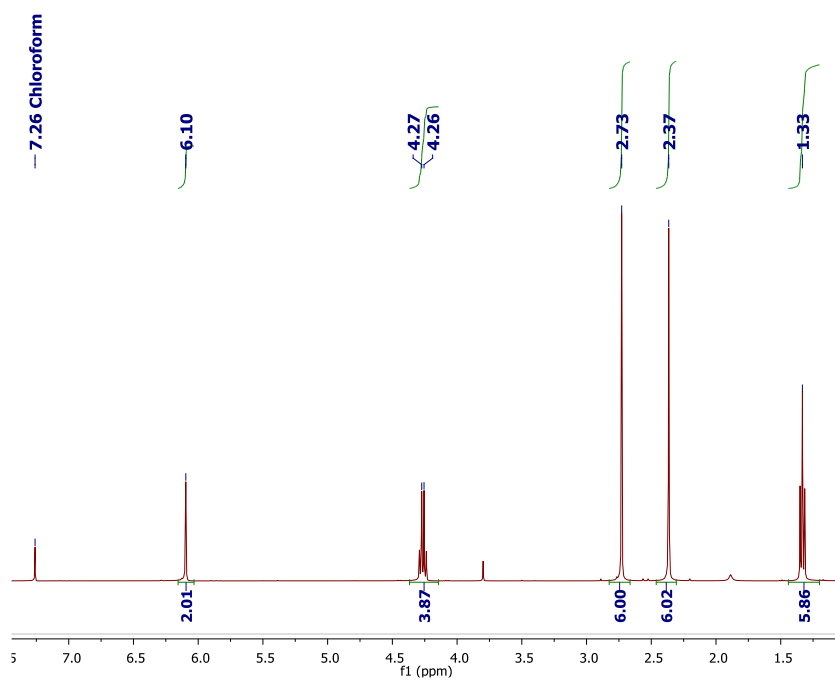


Figure S2: ¹H NMR spectrum of **II** in CDCl₃.

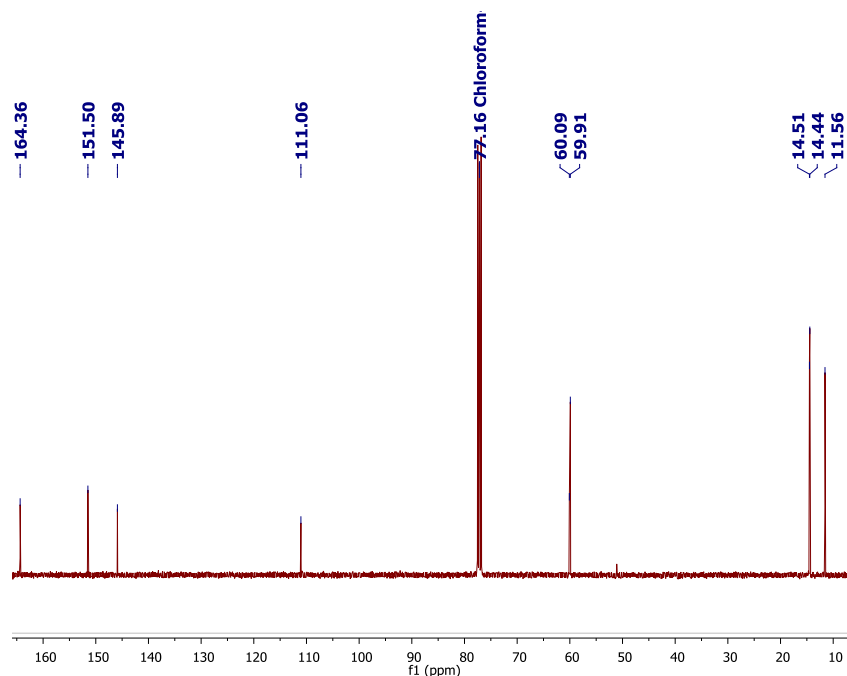


Figure S3: ^{13}C NMR spectrum of **II** in CDCl_3 .

2.3 Synthesis of 1,1'-methylenebis(3,5-dimethyl-1H-pyrazolyl-4-carboxylic acid) (**H₂L**)

II (1.04 g, 2.98 mmol) was combined with freshly ground KOH (1.61 g, 28.8 mmol) in a methanol–water mixture (45 and 5 mL, respectively) and heated overnight at 90 °C. The resulting clear yellow solution was quenched with 12 M hydrochloric acid (2.40 mL, 28.8 mmol) resulting in the precipitation of white solids. The solvent was removed under vacuum and the white solids were suspended in water, collected via vacuum filtration and washed four times with water to yield 2.10 g of the crude material that contains salts. Pure crystals suitable for elemental analysis and MOF synthesis were obtained via the slow diffusion of water into a saturated DMSO solution at 65 °C. The yield of the first crop was 240 mg (28% yield). More product can be obtained by repeating the crystallization process. ^1H NMR (400 MHz, $\text{DMSO-}d_6$) δ 12.32 (s, 2H), 6.23 (s, 2H), 2.67 (s, 6H), 2.24 (s, 6H). ^{13}C NMR (101 MHz, $\text{DMSO-}d_6$) δ 165.00, 150.22, 145.26, 110.11, 58.85, 14.04, 10.88. Anal. Calcd. for $\text{C}_{13}\text{H}_{16}\text{N}_4\text{O}_4$: C 53.42, H 5.52, N 19.17; found C 53.25, H 5.56, N 19.29.

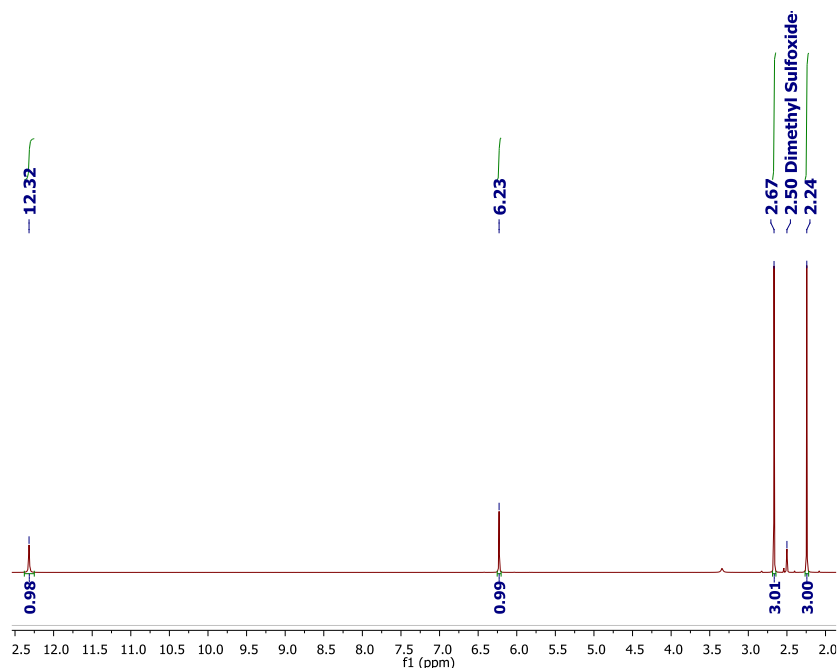


Figure S4: ^1H NMR spectrum of H_2L in $\text{DMSO-}d_6$.

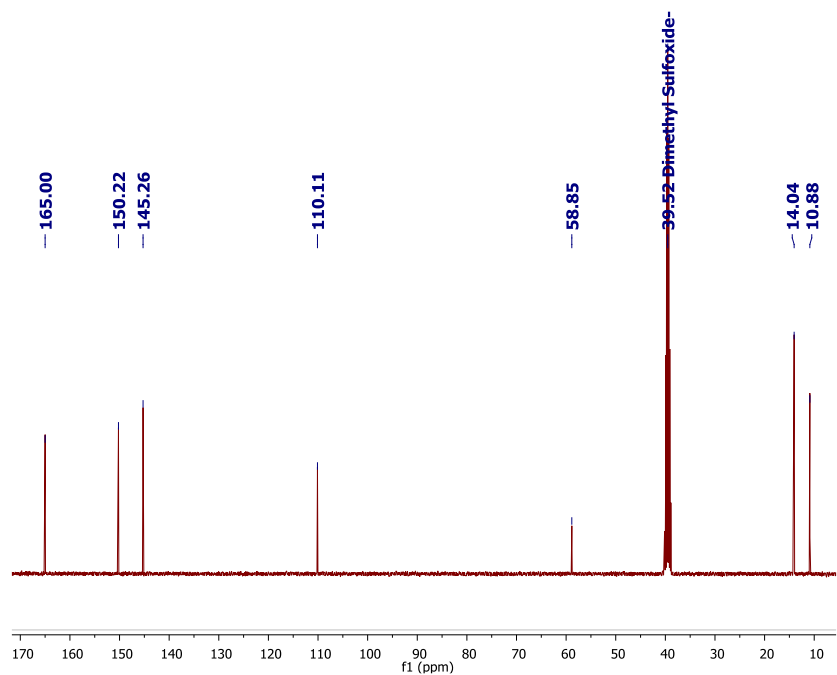


Figure S5: ^{13}C NMR spectrum of H_2L in $\text{DMSO-}d_6$.

2.4 Synthesis of $[\text{NiL}]_n \cdot x\text{DMSO}$ (**1**)

Solutions of H_2L (340 mg, 1.163 mmol) in 17 mL of DMSO and $\text{Ni}(\text{OAc})_2 \cdot 4\text{H}_2\text{O}$ (289 mg, 1.163 mmol) in DMF (6.8 mL) and methanol (1.7 mL) were prepared. 1 mL of H_2L solution was added

to 2-dram scintillation vials and 0.5 mL of nickel solution was syringed on top. The vials were sealed and left to heat at 110 °C for five days in an aluminum block. After heating, X-ray quality electric lime green crystals were collected by vacuum filtration, washed with DMSO, and vacuum dried (332 mg, 63% yield). Elemental analysis of the vacuum dried sample showed 1.35 DMSO molecules per Ni atom, which is consistent with the TGA results for the same sample (Fig S5). Anal. Calc. for $\text{NiC}_{13}\text{H}_{14}\text{N}_4\text{O}_4 \cdot (\text{C}_2\text{H}_6\text{SO})_{1.35}$: C 41.49, H 4.90, N 12.33; found C 41.13, H 4.40, N 11.88.

3 Single Crystal X-Ray Diffraction

3.1 Methods

X-ray quality single crystals were obtained as described in the synthesis above. The crystals were mounted on the tip of a MiTeGen MicroMount. The single-crystal X-ray diffraction data were collected on a Bruker Kappa Apex II Duo CCD diffractometer with Cu $K\alpha$ radiation ($\lambda = 1.54178 \text{ \AA}$) operating at 45 kV and 0.65 mA at 150 K controlled by an Oxford Cryostream 700 series system. The diffraction data was processed with the Bruker Apex 2 software package.⁴ The structure was solved by direct methods and refined using SHELXTL V2016/6.^{5,6} The diffuse electron density of disordered lattice solvent molecules was removed using the Squeeze function of Platon.⁷ The solvent molecules were not included in the formula. All non-hydrogen atoms were refined anisotropically. The positions of the hydrogen atoms were calculated using the riding model.

3.2 Single Crystal Properties

Table S1: Selected crystallographic data for **1**.

Formula	$\text{C}_{208}\text{H}_{224}\text{N}_{64}\text{Ni}_{16}\text{O}_{64}$
Formula Weight [g/mol]	5583.86
Crystal System	Tetragonal
Space Group	$I4_1/a$
a [\AA]	19.5487(6)
b [\AA]	19.5487(6)
c [\AA]	29.888(2)
Volume [\AA^3]	11421.7(9)
Z	1
D(calc) [g/cm^3]	0.812
$\mu(\text{CuK}\alpha)$ [1/mm]	1.099
F(000)	2847
Temperature (K)	147(2)
R_1 and wR_2 for [$I > 2.0 \sigma(I)$]	0.1251, 0.2796
Goof	1.022

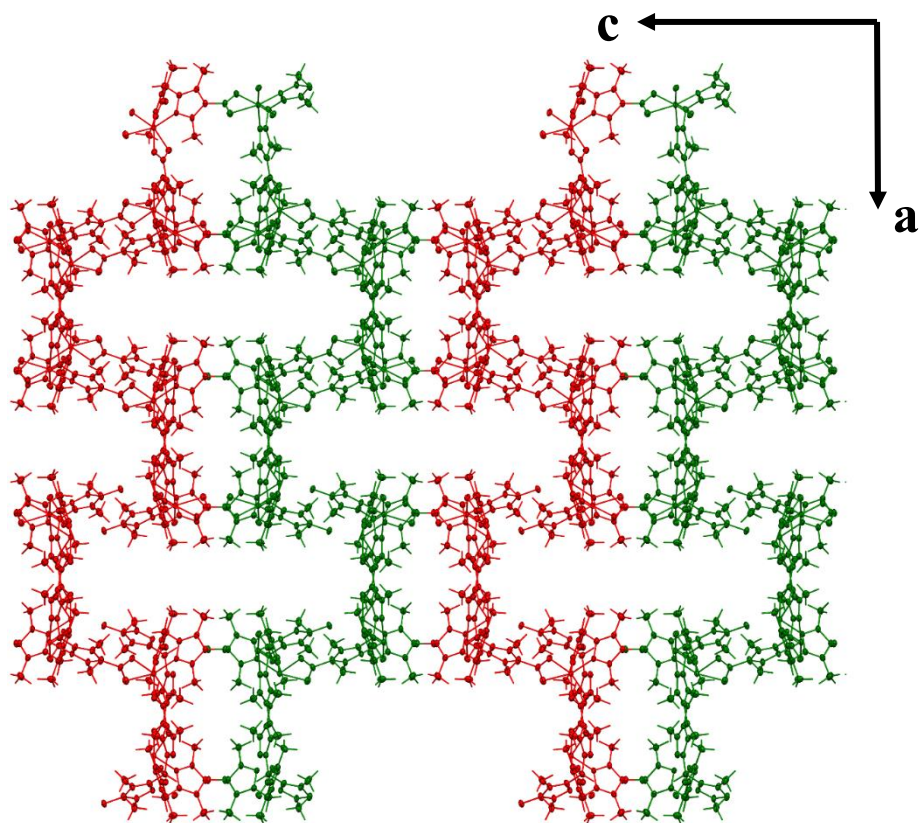


Figure S6: The lattice of **1** viewing down the b axis, showing how the neighbouring chains are linked together through edge-sharing of adjacent squares; the individual chains are colour coded in alternating red and green to match with the colouring convention in Fig. 1f.

4 Thermogravimetric Analysis, Powder X-Ray, and IR

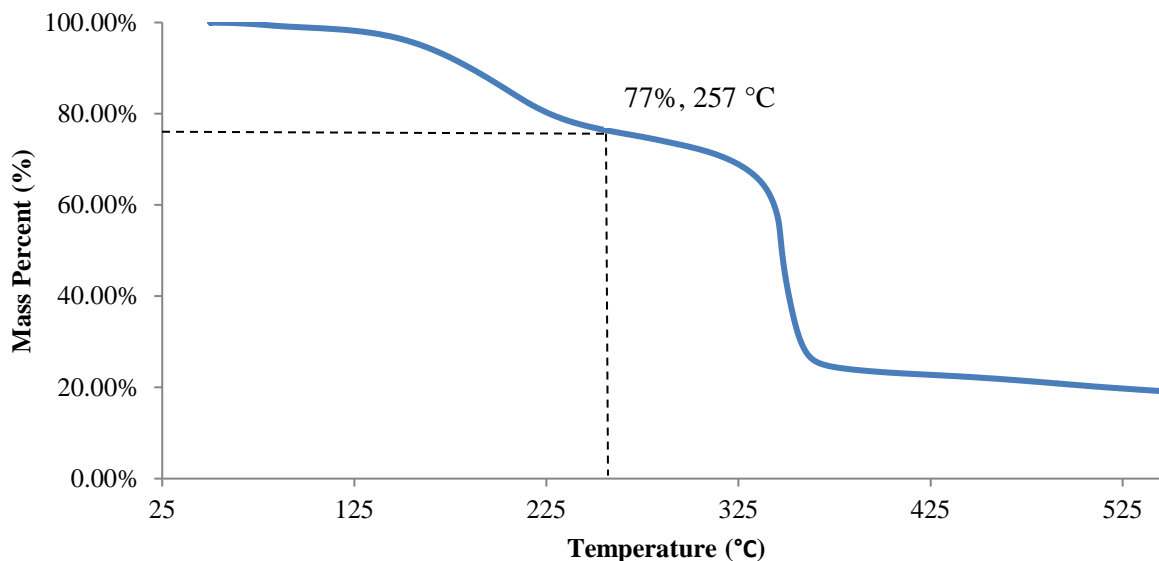


Figure S7: TGA spectrum of partially dried **1**. The weight loss is consistent with the loss of all residual lattice DMSO, based on the composition deduced from elemental analysis ($\text{NiC}_{13}\text{H}_{14}\text{N}_4\text{O}_4 \cdot (\text{DMSO})_{1.35}$).

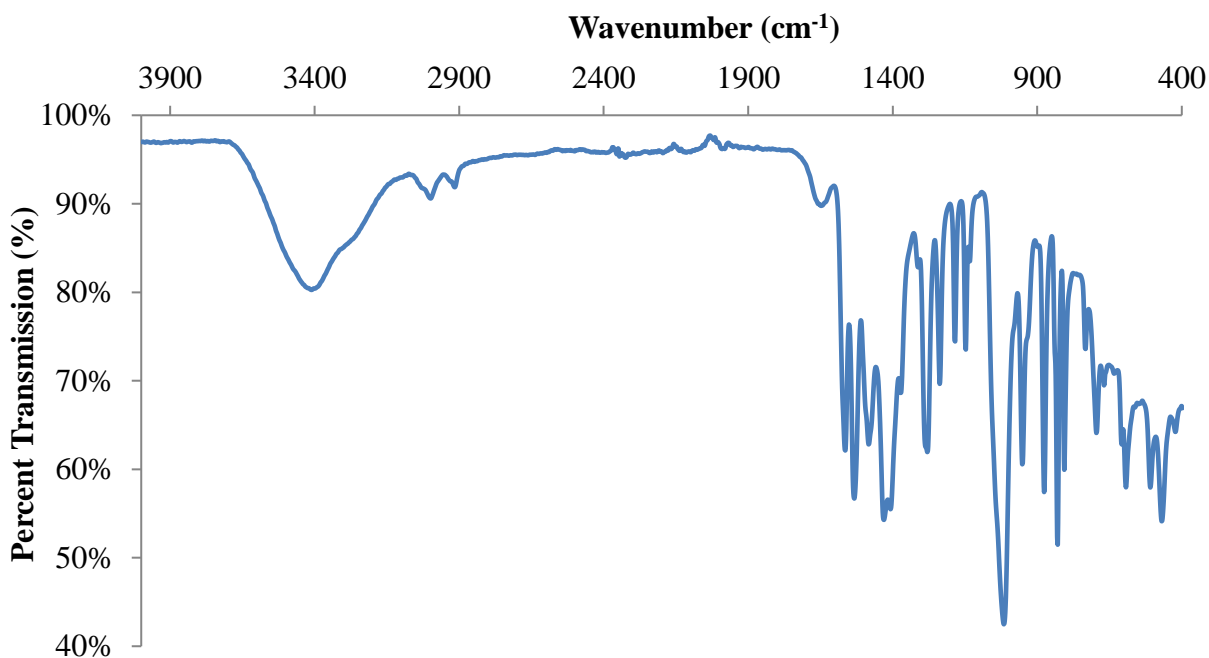


Figure S8: IR Spectrum of neat $[\text{NiL}]_n \cdot x\text{DMSO}$ MOF (**1**).

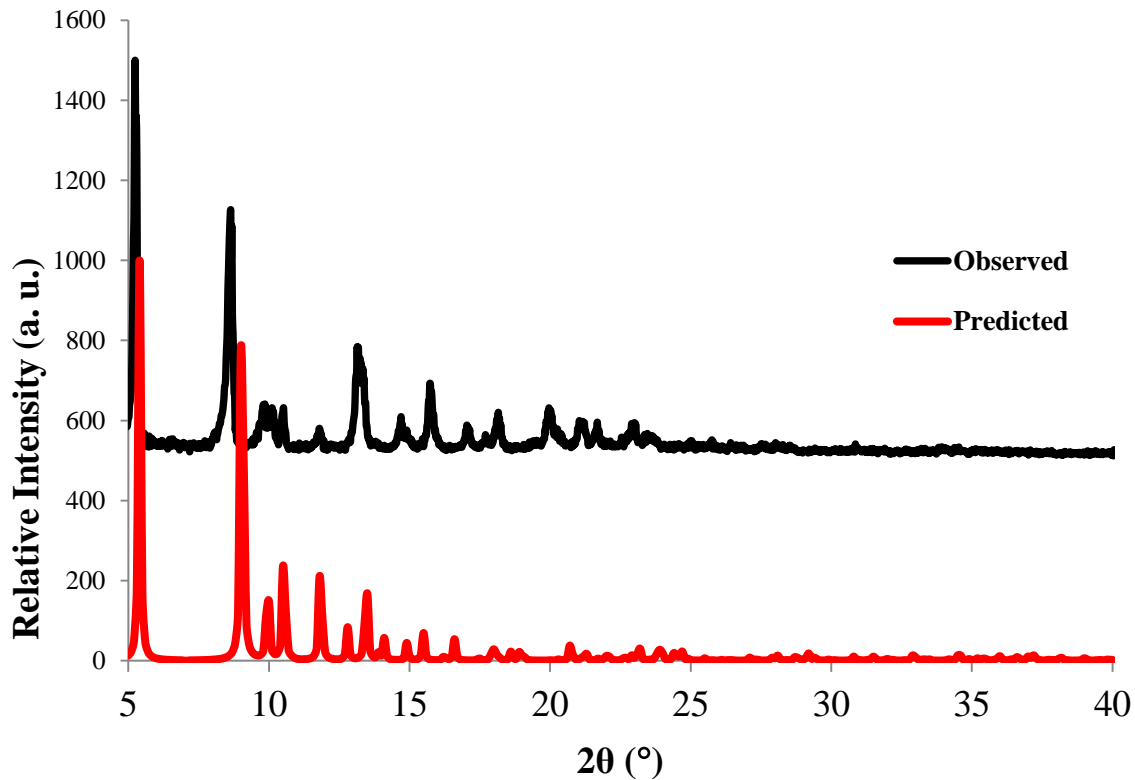


Figure S9: PXRD pattern of as-synthesized MOF **1** vs predicted pattern from single crystal data. The discrepancy is likely due to the “breathing effect” and temperature difference (i.e., 298 K vs 150 K).

5 Gas Sorption

5.1 Adsorption Analysis

1 was prepared for gas sorption analyses by exchanging the lattice solvent with methanol (i.e., soaking with ~15 mL of fresh methanol for 3 h each time for three times) and then with chloroform (soaking with ~15 mL of fresh chloroform overnight each time for three times). The solvent was then decanted and the solid was dried under vacuum ($\sim 10^{-3}$ mbar) for 90 minutes before being backfilled with argon. Finally, the sample was activated on the ASAP2020 instrument for 2 h at 60 °C followed by 16 h at 100 °C, at which point no further outgassing was observed. The sample was then backfilled with N₂ before being transferred to the analysis port, where it was evacuated for another 2 h before the analysis.

5.2 Surface Area

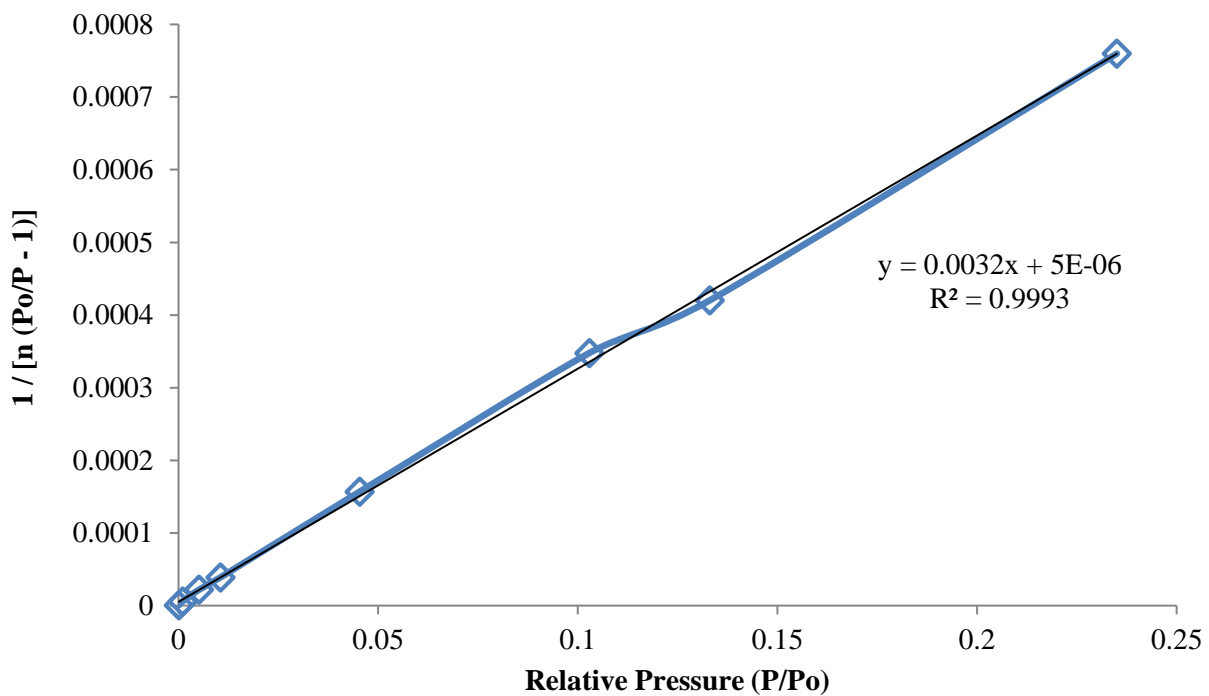


Figure S10: BET plot and fit for **1** adsorbing N_2 at 77 K.

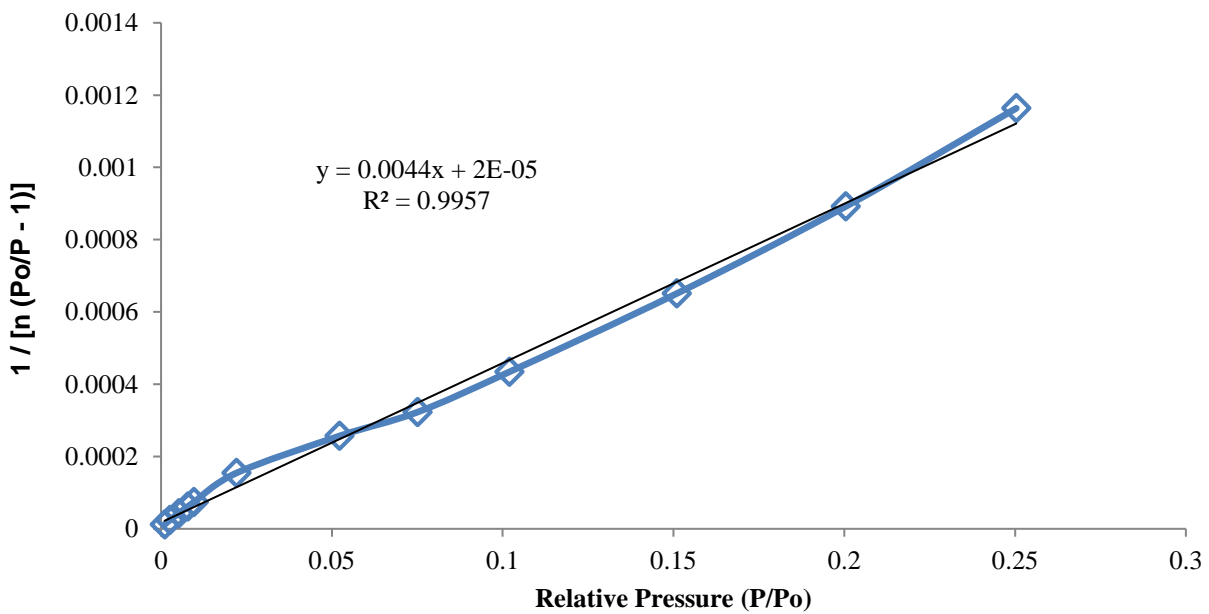


Figure S11: BET plot and fit for **1** adsorbing CO_2 at 195 K.

5.3 Isothermic Heat of Adsorption Calculation

From Dual-Site Langmuir isotherm fitting, a modified Clausius-Clapeyron equation was used with all six temperatures to determine the heat of adsorption (ΔH_{ads}) for CH_4 , CO_2 , and N_2 .⁸

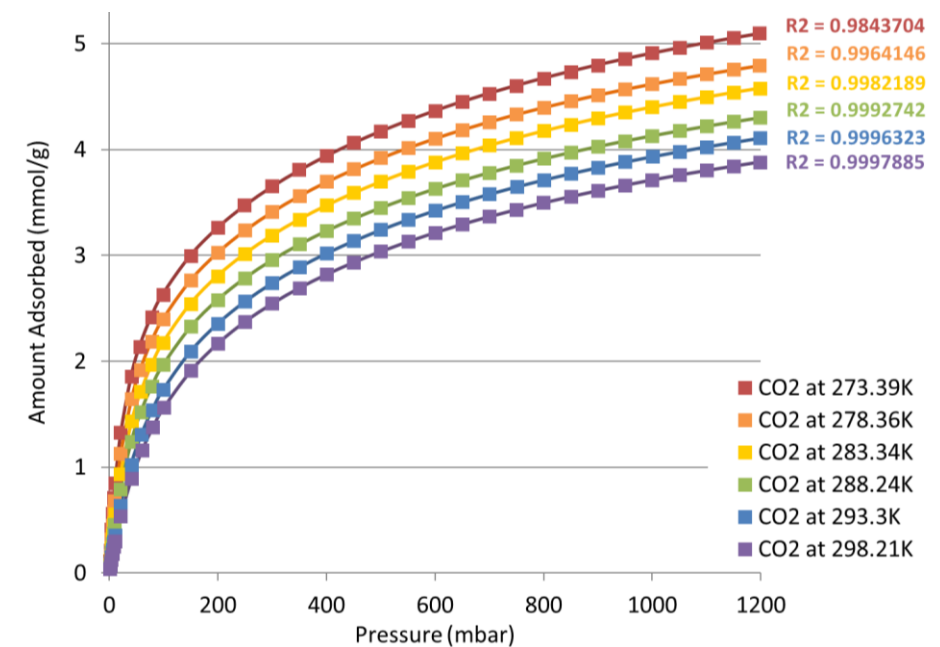


Figure S12: CO_2 sorption isotherms (squares) and fits (solid lines) for **1**.

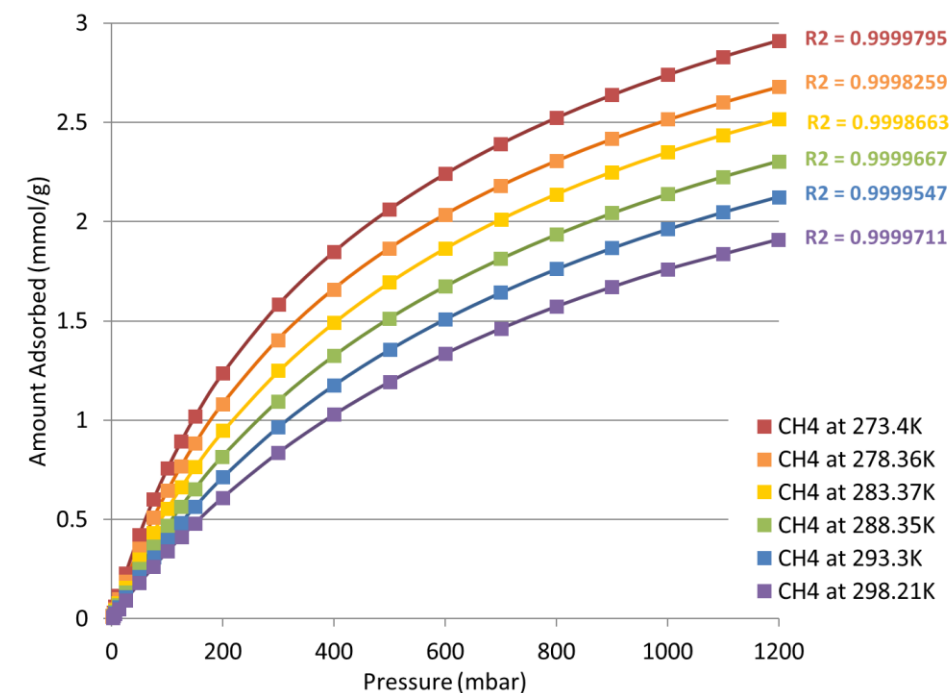


Figure S13: CH_4 sorption isotherms (squares) and fits (solid lines) for **1**.

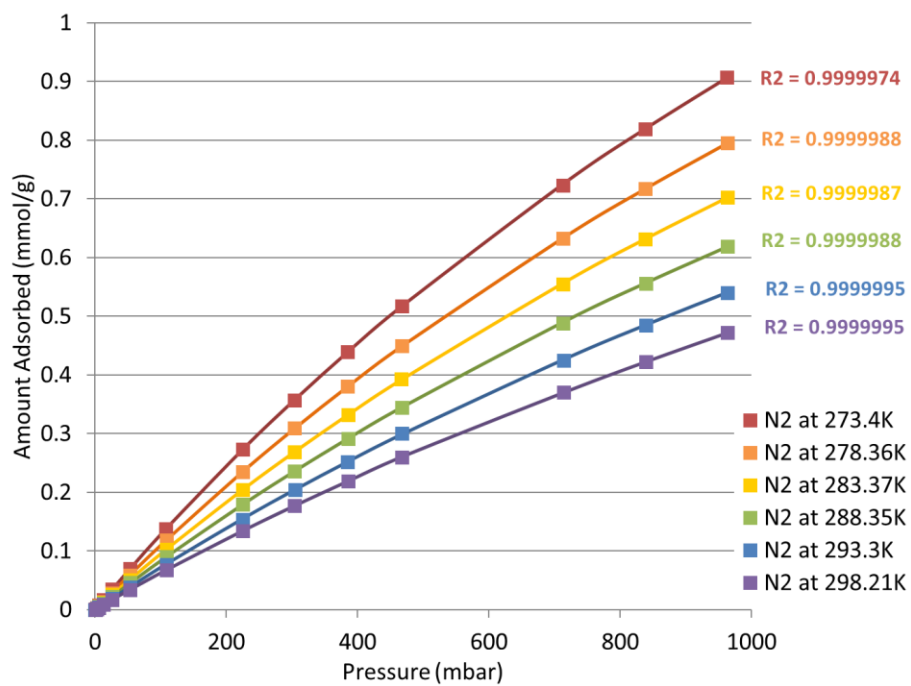


Figure S14: N₂ sorption isotherms (squares) and fits (solid lines) for **1**.

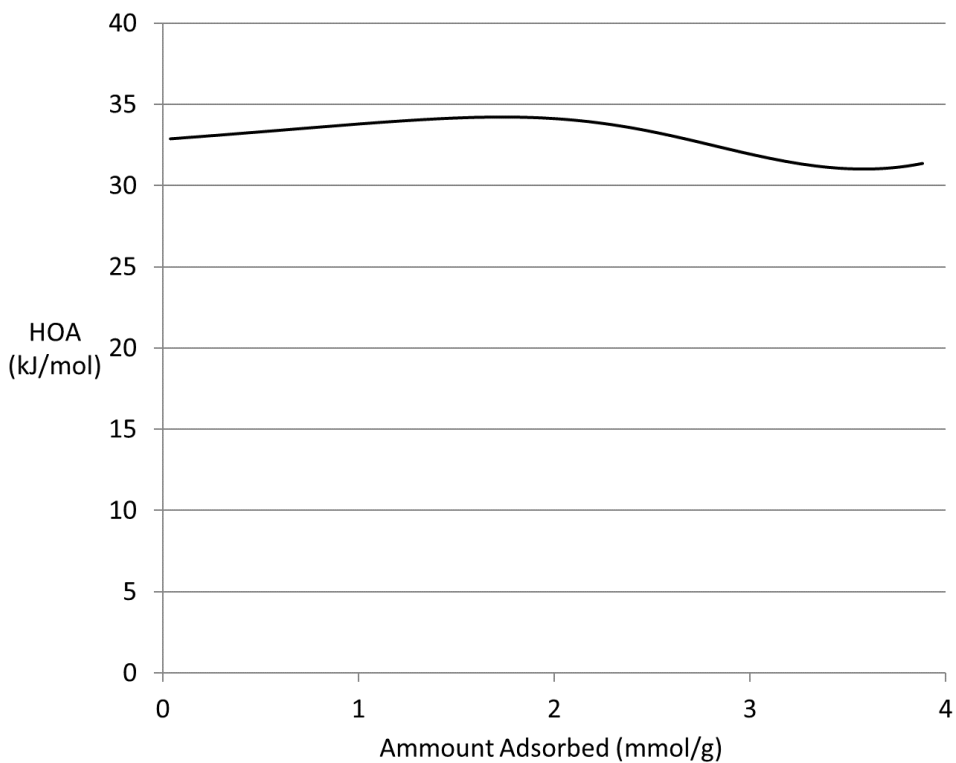


Figure S15: Enthalpy of absorption of **1** for CO₂.

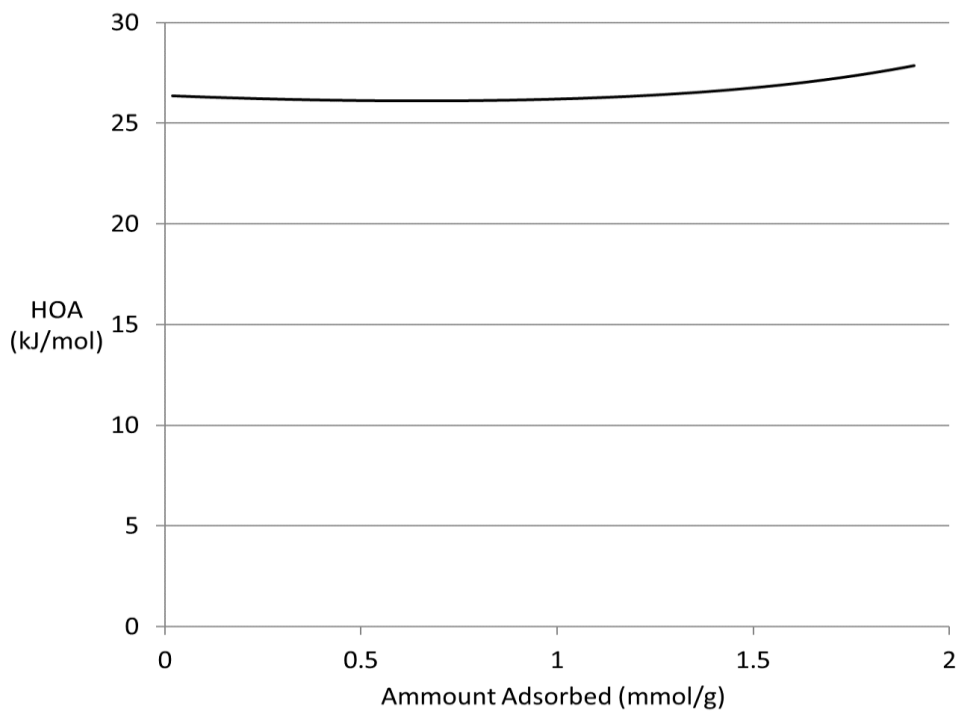


Figure S16: Enthalpy of absorption of **1** for CH₄.

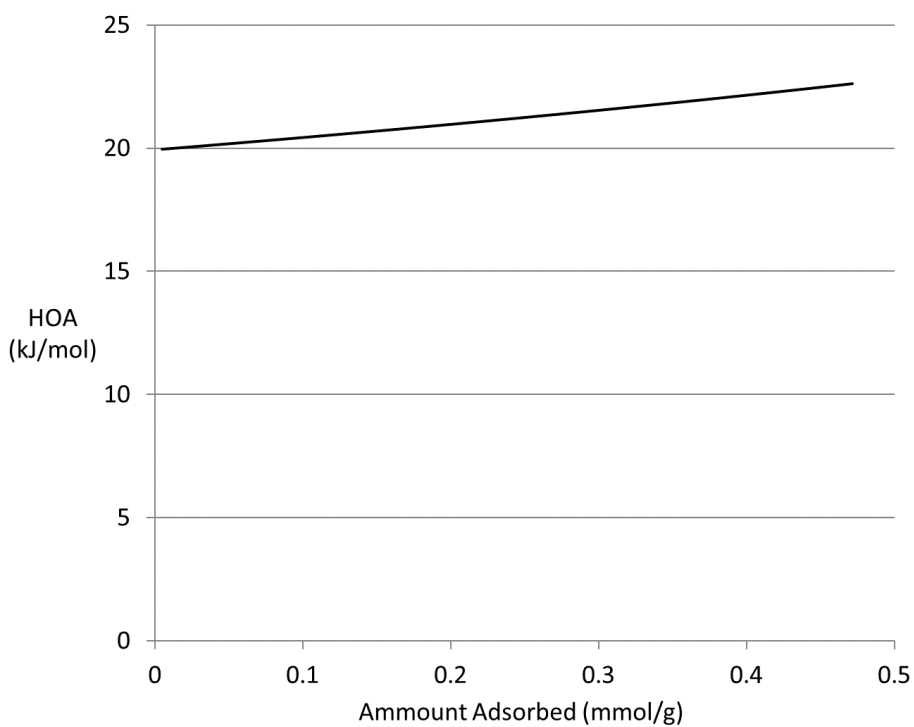


Figure S17: Enthalpy of absorption of **1** for N₂.

5.4 Selectivity

Selectivity was calculated by fitting the single component isotherms to a Dual-Site Langmuir model and then by using Ideal Adsorbed Solution Theory (IAST) via pyIAST.^{9,10}

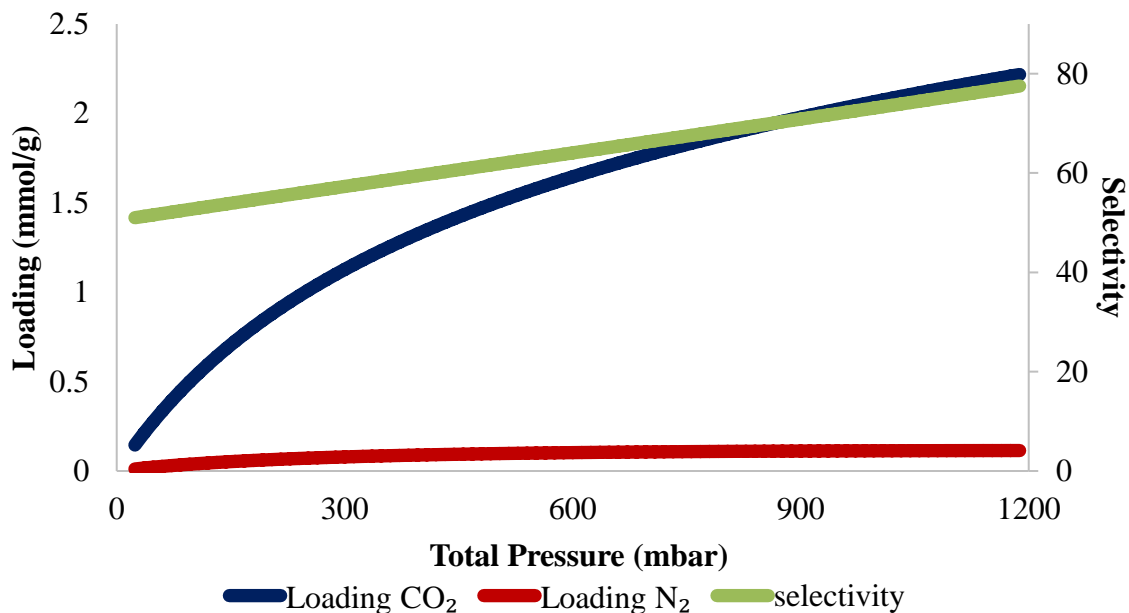


Figure S18: IAST determined selectivity for a 20% CO₂/80% N₂ gas stream at 298K adsorbing onto **1**.

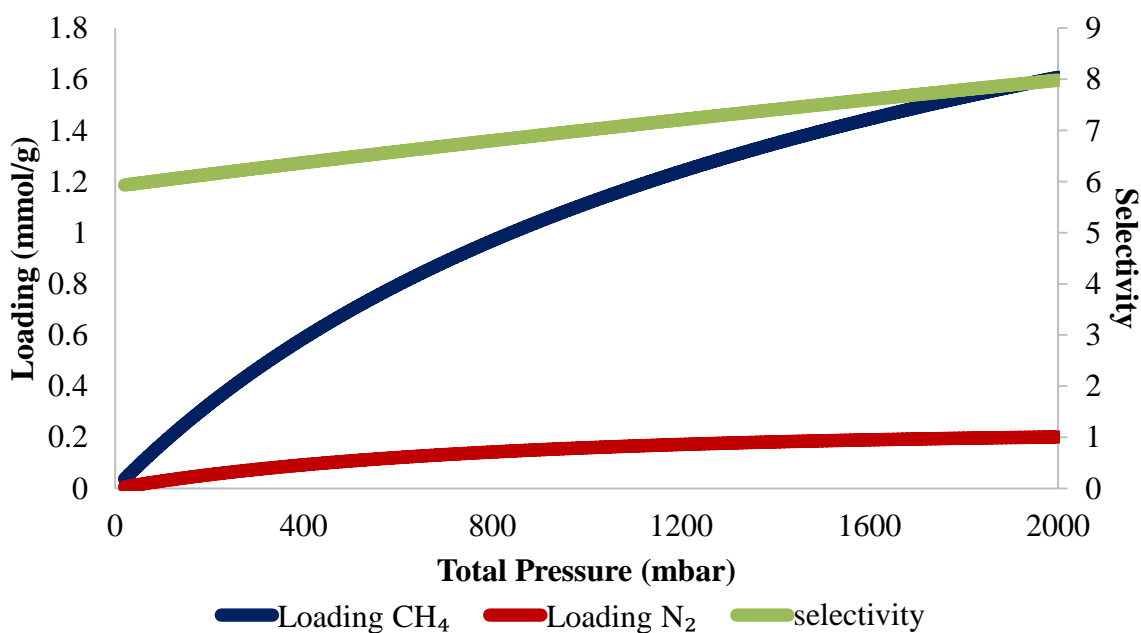


Figure S19: IAST determined selectivity for a 1:1 mixture of CH₄/N₂ at 298K adsorbing onto **1**.

5.5 Selectivity and Working Capacity Comparison of **1** versus other Literature Materials

Table S2: Selectivity and working capacity data of literature MOFs and similar materials in comparison to **1**. Selectivity data are reported for 1 bar of pressure at 298 K and working capacity is for the pressure range of 0.2–1.0 bar.

Name	Selectivity at 1 bar	Working Capacity (mmol/g)	Reference
1	7.0	1.15	This Work
[Cu(INA) ₂] _n	6.9	~0.60 ^a	11
[Ni ₃ (HCOO) ₆] _n	6.2	~0.60 ^a	11
Al-BDC ^b	3.0	~0.50 ^a	11
Ni-MOF-74 ^c	1.4	~2.0 ^a	11
ZIF-7 ^d	4	0.41	12
Cu-MOF ^e	6.9	~0.3 ^a	13
ROD-8 ^f	~9	~0.45 ^a	14
[Mg ₃ (HCOO) ₆] _n	4.8 ^g	~0.55 ^a	15
[Mn ₃ (HCOO) ₆] _n	4.1 ^g	~0.40 ^a	15
[Co ₃ (HCOO) ₆] _n	5.6 ^g	~0.55 ^a	15
MIL-101 (Cr) ^h	2.22 ⁱ	~1.2 ^{a,i}	16
³ ∞[Cu(Me-4py-trz-ia)] ^j	4.2	N/A	17
MOF-5 ^k	1.13	~0.10 ^a	18
MOF-177 ^l	4.00	~0.65 ^a	18
Zeolite 5A	0.94	~0.95	18

^a Data extracted from reported gas sorption isotherms; ^b Al-BDC is [Al(BDC)(OH)]_n, where BDC is 1,4-benzenedicarboxylate; ^c Ni-MOF-74 is Ni₂(dhtp)(H₂O)₂·8H₂O where H₄dhtp is 2,5-dihydroxyterephthalic acid; ^d ZIF-7 is [Zn(BIM)]_n, BIM = benzimidazolidine; ^e Cu-MOF is Cu(hfipbb)(H₂hfipbb)_{0.5}, where H₂hfipbb is 4,4'-(hexafluoro-isopropylidene)bis(benzoic acid); ^f ROD-8 is [Cd₂(TBAPy)(H₂O)₂]·DMF·0.5dioxane, where TBAPy = 1,3,6,8-tetrakis(*p*-benzoate)pyrene; ^g Selectivity reported at 0.4 MPa; ^h MIL-101(Cr) is [Cr₃F(H₂O)₂O(BDC)₃·*n*H₂O]_n; ⁱ Values reported at 303 K; ^j Me-4py-trz-ia is 5-(3-methyl-5-(pyridin-4-yl)-4*H*-1,2,4-triazol-4-yl)isophthalate; ^k MOF-5 is [Zn₄O(BDC)]_n; ^l MOF-177 is [Zn₄O(BTB)]_n, where BTB is benzene tribenzoate.

5.6 Post Adsorption Stability

Post-adsorption TGA was performed using a NETZSCH STA 409PC Luxx. The sample was loaded into the aluminum sample carrier, with an empty aluminum sample carrier as a reference. The sample was then heated to 450 °C at 2 °C min⁻¹.

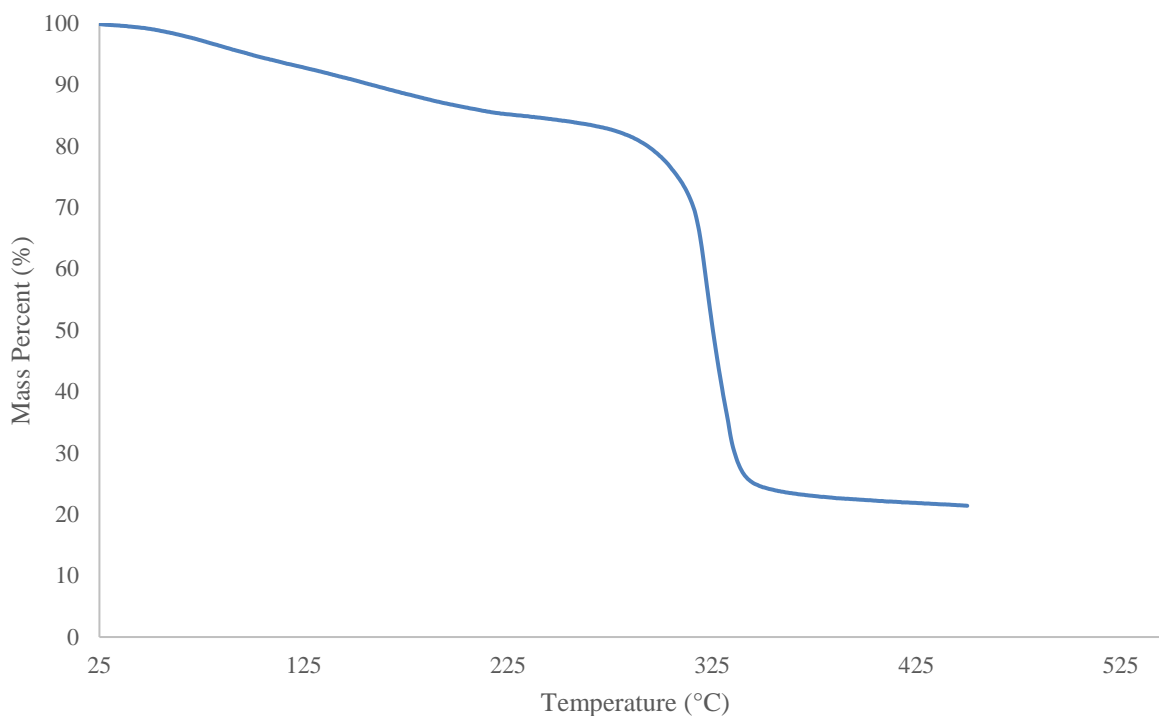


Figure S20: Post-adsorption TGA of **1** showing that the stability of the framework remains similar to the as-synthesized **1**.

6 Stability of **1**

6.1 Chemostability of **1**

1 is stable in common laboratory solvents such as acetone, DMSO, chloroform, DMF, and methanol. No precautions were taken against moisture. Qualitative testing with water shows full dissolution of **1** in pure distilled water over 24 hours.

6.2 Thermal stability of **1**

In order to assess the long-term stability of **1** the PXRD experiment was performed on a sample that was stored in air for 18 months at ambient temperature. The results (Figure S21) show that the

MOF in general is relatively stable. However, the structural change caused by the “breathing effect” is evident, i.e., the PXRD pattern of the old sample is different from that of a fresh sample of **1**, presumably caused by the exchange of channel content with ambient lab air over 18 months. Interestingly, when this aged sample of **1** is heated to 100 °C (i.e., the same temperature used for sample activation right before the gas adsorption measurements) to release the extraneous guest molecules, the PXRD pattern shows a better match with the simulated pattern based on single crystal diffraction data (Figure S22), supporting our hypothesis of the “breathing effect”. VT-PXRD shows that **1** remains crystalline at 200 °C.

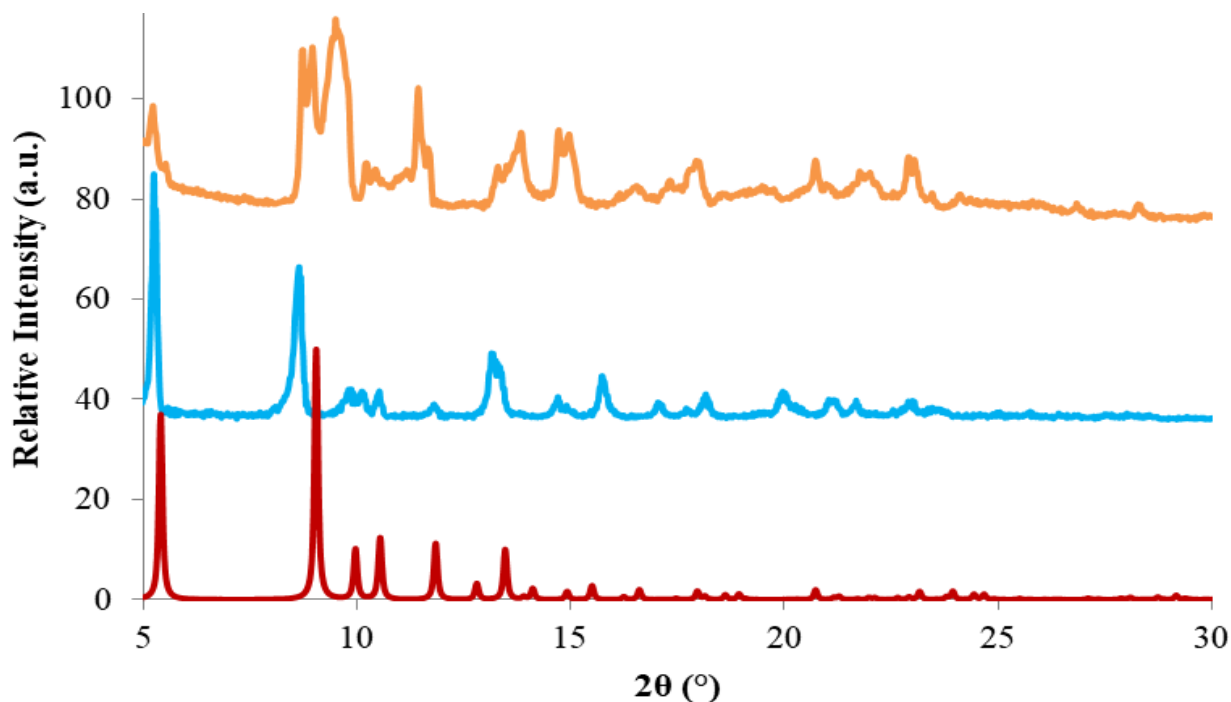


Figure S21: The PXRD patterns of fresh (blue) and aged (orange) **1** and the simulated PXRD pattern (red) of **1** based on the single crystal X-ray diffraction data obtained at 150 K.

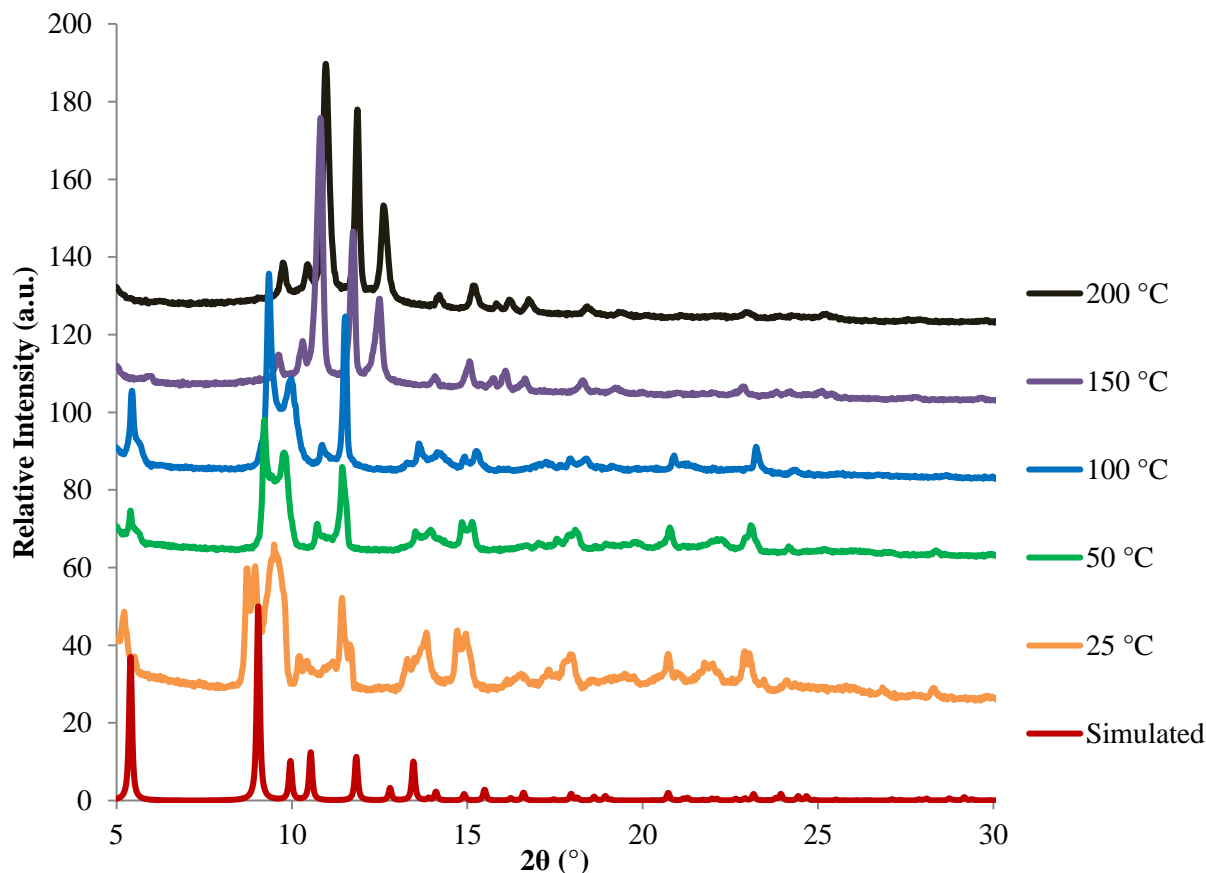


Figure S22: The PXRD patterns of an aged sample of **1** at 25~200 °C in comparison with the PXRD pattern simulated based on the single crystal X-ray diffraction data at 150 K.

7 Computational Details and Observed CH₄ and N₂ Sites of Adsorption in **1**

In order to investigate the observed selective adsorption in **1**, the preferred binding sites for CH₄ and N₂ in the evacuated MOF were determined using Grand Canonical Monte Carlo (GCMC) calculations. These simulations were performed with an in-house developed code¹⁹ based on the DL_POLY Classic code²⁰ in which the MOF framework was fixed. GCMC gas adsorption simulations for pure CH₄ and N₂ were carried out isothermally at 298 K with adsorption pressures of up to 2 bar. The GCMC simulations were run for 1,000,000 equilibration steps and 15,000,000 production steps each. To generate the probability distributions, GCMC simulations of 2×10^8 steps were taken. The positions of framework atoms in **1** were taken from single crystal XRD data, with the hydrogen atom positions being optimized at the DFT level. The Lennard-Jones (LJ) potentials were used to model the van der Waals non-bonding steric and dispersion interactions and the partial atomic charge approximation with E_{wald} summations were used for the long-range electrostatic interactions. The LJ parameters for the MOF framework were taken from the universal force field (UFF) force field.²¹ Partial atomic charges were calculated using the REPEAT

method which provide charges that best fit the electrostatic potential resulting from a periodic DFT calculation.²² Periodic DFT calculation were performed using the VASP^{23,24} package with the PBE²⁵ functional and a planewave cut-off a 520 eV. The LJ parameters for CH₄ and N₂ guest molecules were taken from the CH₄-TraPPE²⁶ and N₂-TraPPE²⁷ force fields.

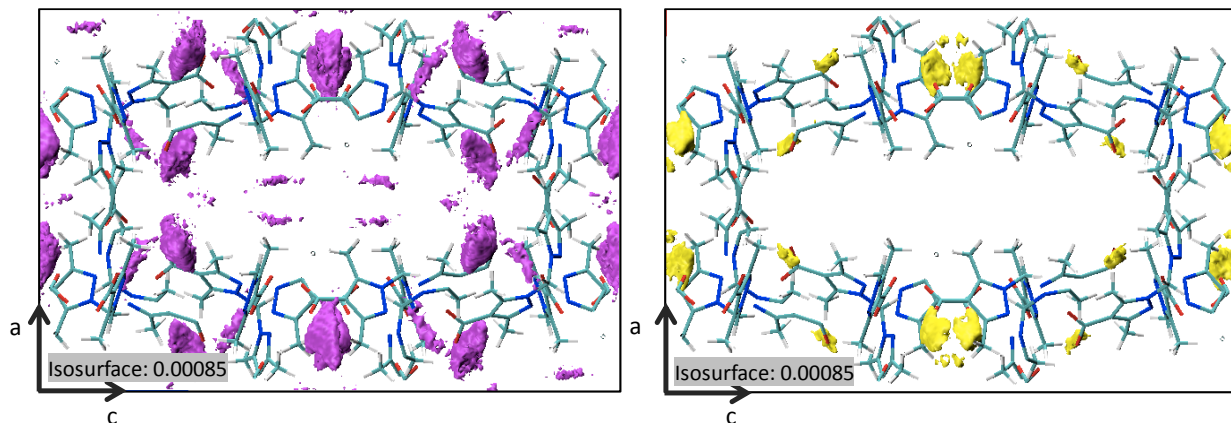


Figure S23: a) Isosurface plots of the N₂ center of mass probability density in a unit cell of **1** from a) a binary simulation of CH₄/N₂ at a 1:1 ratio at 298 K and total pressure of 1 bar and from b) a single component GCMC simulation of N₂ at 298 K and 0.5 bar.

8 References

- 1 M. W. Rathke and P. J. Cowan, *J. Org. Chem.*, 1985, **50**, 2622–2624.
- 2 J.-C. Jung, E. B. Watkins and M. A. Avery, *Tetrahedron*, 2002, **58**, 3639–3646.
- 3 L. D. Field, B. A. Messerle, M. Rehr, L. P. Soler and T. W. Hambley, *Organometallics*, 2003, **22**, 2387–2395.
- 4 *Apex 2 Software Package*, Bruker AXS Inc., Madison, WI, 2013.
- 5 G. M. Sheldrick, *Acta Crystallogr. A*, 2008, **64**, 112–122.
- 6 The SHELX homepage, <http://shelx.uni-ac.gwdg.de/SHELX/index.php>, (accessed 17 May 2017).
- 7 A. L. Spek, *J. Appl. Crystallogr.*, 2003, **36**, 7–13.
- 8 J.-S. Lee, J.-H. Kim, J.-T. Kim, J.-K. Suh, J.-M. Lee and C.-H. Lee, *J. Chem. Eng. Data*, 2002, **47**, 1237–1242.
- 9 A. L. Myers and J. M. Prausnitz, *AIChE J.*, 1965, **11**, 121–127.

- 10 C. M. Simon, B. Smit and M. Haranczyk, *Comput. Phys. Commun.*, 2016, **200**, 364–380.
- 11 J. Hu, T. Sun, X. Liu, Y. Guo and S. Wang, *RSC Adv.*, 2016, **6**, 64039–64046.
- 12 A. Arami-Niya, G. Birkett, Z. Zhu and T. E. Rufford, *J. Mater. Chem. A*, , DOI:10.1039/C7TA03755D.
- 13 X. Wu, B. Yuan, Z. Bao and S. Deng, *J. Colloid Interface Sci.*, 2014, **430**, 78–84.
- 14 R.-J. Li, M. Li, X.-P. Zhou, S. Weng Ng, M. O’Keeffe and D. Li, *CrystEngComm*, 2014, **16**, 6291–6295.
- 15 J. Hu, T. Sun, X. Liu, S. Zhao and S. Wang, *Microporous Mesoporous Mater.*, 2016, **225**, 456–464.
- 16 K. Munusamy, G. Sethia, D. V. Patil, P. B. Somayajulu Rallapalli, R. S. Somani and H. C. Bajaj, *Chem. Eng. J.*, 2012, **195–196**, 359–368.
- 17 J. Möllmer, M. Lange, A. Möller, C. Patzschke, K. Stein, D. Lässig, J. Lincke, R. Gläser, H. Krautscheid and R. Staudt, *J. Mater. Chem.*, 2012, **22**, 10274–10286.
- 18 D. Saha, Z. Bao, F. Jia and S. Deng, *Environ. Sci. Technol.*, 2010, **44**, 1820–1826.
- 19 P. G. Boyd, PhD thesis, University of Ottawa, 2015.
- 20 W. Smith and T. R. Forester, *J. Mol. Graph.*, 1996, **14**, 136–141.
- 21 A. K. Rappe, C. J. Casewit, K. S. Colwell, W. A. Goddard and W. M. Skiff, *J. Am. Chem. Soc.*, 1992, **114**, 10024–10035.
- 22 C. Campañá, B. Mussard and T. K. Woo, *J. Chem. Theory Comput.*, 2009, **5**, 2866–2878.
- 23 G. Kresse and J. Hafner, *Phys. Rev. B*, 1993, **47**, 558–561.
- 24 G. Kresse and J. Hafner, *Phys. Rev. B*, 1994, **49**, 14251–14269.
- 25 J. P. Perdew, K. Burke and M. Ernzerhof, *Phys. Rev. Lett.*, 1996, **77**, 3865–3868.
- 26 M. G. Martin and J. I. Siepmann, *J. Phys. Chem. B*, 1998, **102**, 2569–2577.
- 27 J. J. Potoff and J. I. Siepmann, *AIChE J.*, 2001, **47**, 1676–1682.